ARTICLE

Print path-dependent contact temperature dependency for 3D printing using fused filament fabrication

Yao Xu[1] | Miaozi Huang[1] | Alois K. Schlarb[1,2,3]

[1]Chair of Composite Engineering (CCe), Technische Universität Kaiserslautern (TUK), Kaiserslautern, Germany

[2]Research Center OPTIMAS, Technische Universität Kaiserslautern (TUK), Kaiserslautern, Germany

[3]Qingdao University of Science & Technology, Qingdao, China

Correspondence
Alois K. Schlarb, Chair of Composite Engineering (CCe), Technische Universität Kaiserslautern (TUK), Gottlieb-Daimler-Str. Bld. 44, 67663 Kaiserslautern, Germany.
Email: alois.schlarb@mv.uni-kl.de

Abstract

This paper focuses on the effects of different time spans and thus different contact temperatures when a molten strand contacts an adjacent already solidified strand in a plane during 3D printing with fused filament fabrication. For this purpose, both the manufacturing parameters and the geometry of the component are systematically varied and the effect on morphology and mechanical properties is investigated. The results clearly show that even with identical printing parameters, the transitions between the individual layers are much more visible with long time spans until fusion and lead to low mechanical properties. In contrast, short spans lead to hardly visible welds and high mechanical properties. Transferring the findings to different component sizes ultimately verifies that the average temperature at the time of contact between the already solidified and the currently deposited strand is decisive for component quality. In order to generate high component qualities, this finding must therefore be taken into account in the future in the path generation strategy, i.e., in so-called slicing.

KEYWORDS
fused filament fabrication, mechanical strength, morphology, polypropylene

1 | INTRODUCTION

Fused filament fabrication (FFF) has attracted considerable attention as an effective tool due to its simplicity, low time-to-market, and freedom of design.[1–4] Although it is a decades technology,[5] FFF is one of the methods with the greatest potential to satisfy the design with various geometry of components and deposit multiple parts simultaneously.[6–8] In FFF, a thermoplastic filament is melted in a moving hot nozzle via heat conduction, and then the strand is deposited according to a laying pattern matched to the component. Between the stacked rods, the inter-strand adhesion and interlayer adhesion occurs when the new strand is deposited beside and on the top of a

previously printed strand, respectively.[9] Considering the process, the anisotropy mechanical properties of printed parts originated from the layer-wise strategy and the rapid thermal gradients.[10–12] As such, to overcome the limited mechanical issue of the specimen, the challenge is to optimize the welding behavior during the FFF process.

To obtain high-quality parts, one major aspect is the fusion between the deposited strands.[13] Fusion determines the bond quality between strands and is directly correlated with mechanical properties.[14,15] Adhesion leads to the formation of strong bonds at the interface through the entanglement of polymer chains across the interface.[16] During the deposition of the molten strand, the previously deposited strand cooled to different

temperatures over time. In the weld lines, the temperature affects molecular chain diffusion, which in turn affects the fusion process and adhesion.[17,18] The sufficient thermal energy and longer weld time can form a good interface between strands.[19,20] Therefore, the contact temperature of the weld zone plays an important role in the formation of weld lines. The fusion of the semi-crystalline thermoplastic during melt deposition is governed by crystallization, which limits the interfacial molecular diffusion.[21] When semi-crystalline thermoplastics such as polypropylene (PP) are printed via FFF, these factors are especially crucial because they determine the crystallization behavior, the interfacial fusion, and ultimately determine the mechanical properties.[22,23]

Recently, extensive related studies exist for describing the influence factors on mechanical properties.[24–26] The researches focused on the machine parameters such as the nozzle temperature,[27] the filling density,[28] raster orientation[29] and bed temperature,[30] which are related to the porosity, crystallinity, and mechanical properties of the printed parts. However, the effects of contact time spans on the properties of 3D printed parts have not been exhaustively studied yet. This effect is especially important, as it can optimize the properties of weld lines and design of various geometry of the components manufactured by FFF.

In this work, we printed a special triangle specimen aiming to explore the effect of time spans and printing paths on the morphology and mechanical properties. And the local temperature profiles are measured to reveal their influence on the contact temperature. Further, the micro-tensile strength of samples with different dimensions was studied to obtain the relationship between contact temperature and properties.

2 | MATERIAL AND METHODS

Isotactic polypropylene PP HD 120MO (Borealis GmbH, Burghausen, Germany) with a melt flow rate (MFR) of 8 g/10 min (230°C, 2.16 kg), and the weight-average molecular weight (Mw) of 365 kg/mol, was used in this study. From the pellets, PP filaments with a diameter of $d = 2.8 \pm 0.05$ mm were fabricated via a single screw extruder (EX6, Filabot, Barre, USA). The barrel temperatures for fabricating filaments were selected as 40/130/200/195°C from the hopper to the die. The screw speed was set at 6 rpm.

Two geometries of specimens, namely triangular-shaped specimens (Figure 1a) and cubic specimens (Figure 1b) with specific dimensions, were processed in an FFF 3D printer (Ultimaker 3, Ultimaker B.V., Netherlands) with the printing parameters summarized in Table 1. The

idea to print a triangular specimen is based on the hypothesis that the time to contact between two deposited strands in one plane but also between the planes determines the contact temperature (welding temperature) and thus the morphology and ultimately also influences the mechanical properties in y- and z-direction (perpendicular to the printing direction). The cubic specimens were printed in order to be able to mechanically characterize specimens with different contact times in a simple way.

To avoid warping, the first layer of specimens was printed with a brim on a PP tape (Tesa 64,014). For comparison, injection molded (IM) plates were prepared using the same PP. The temperature for injection molding was set from 170°C near the hopper to 190°C at the nozzle. The mold temperature was 40°C and the injection rate was 10 cm/s.

Printing was started at the coordinate origin ($x = 0$, $y = 0$) and the triangular specimen was built up layer by layer along the meandering path drawn in Figure 1a from the longest side (hypotenuse) to the apex of the triangle. In a section along the plane of symmetry, the areas of confluence between adjacent strands were numbered from I to X. The associated distances traveled (Δl) and time spans to contact (Δt) were calculated according to Equations (1) and (2) and listed in Table 2.

$$\Delta l_i = \frac{L_i}{2} + \frac{L_{i+1}}{2} \tag{1}$$

$$\Delta t_i = \frac{\Delta l_i}{v} \tag{2}$$

where l_i is the length of the strand, l_{i+1} is the length of the adjacent strand, and v is the printing speed.

To investigate the morphology, the prepared A-A cross section of triangular-shaped samples were cut by a rotation microtome (Hyrax M 25, Carl Zeiss, MicroImaging GmbH, Jena, Germany) equipped with a steel blade and then chemically etched in a chemical solution, which contained potassium permanganate, sulfuric acid and phosphoric acid.[31,32] The chemically etched surfaces were then inspected using an optical microscope (OM) (Nikon ECLIPSE LV100POL, Nikon GmbH, Düsseldorf, Germany).

The thermal properties of the printed samples were analyzed under a 50 ml min^{-1} nitrogen gas flow using a differential scanning calorimetry (DSC Q20, TA Instruments, USA). The investigations were performed from 40 to 200°C with a heating/cooling rate of 10°C/min. The degree of crystallinity X_c for the PP phase was determined by using the following equation:

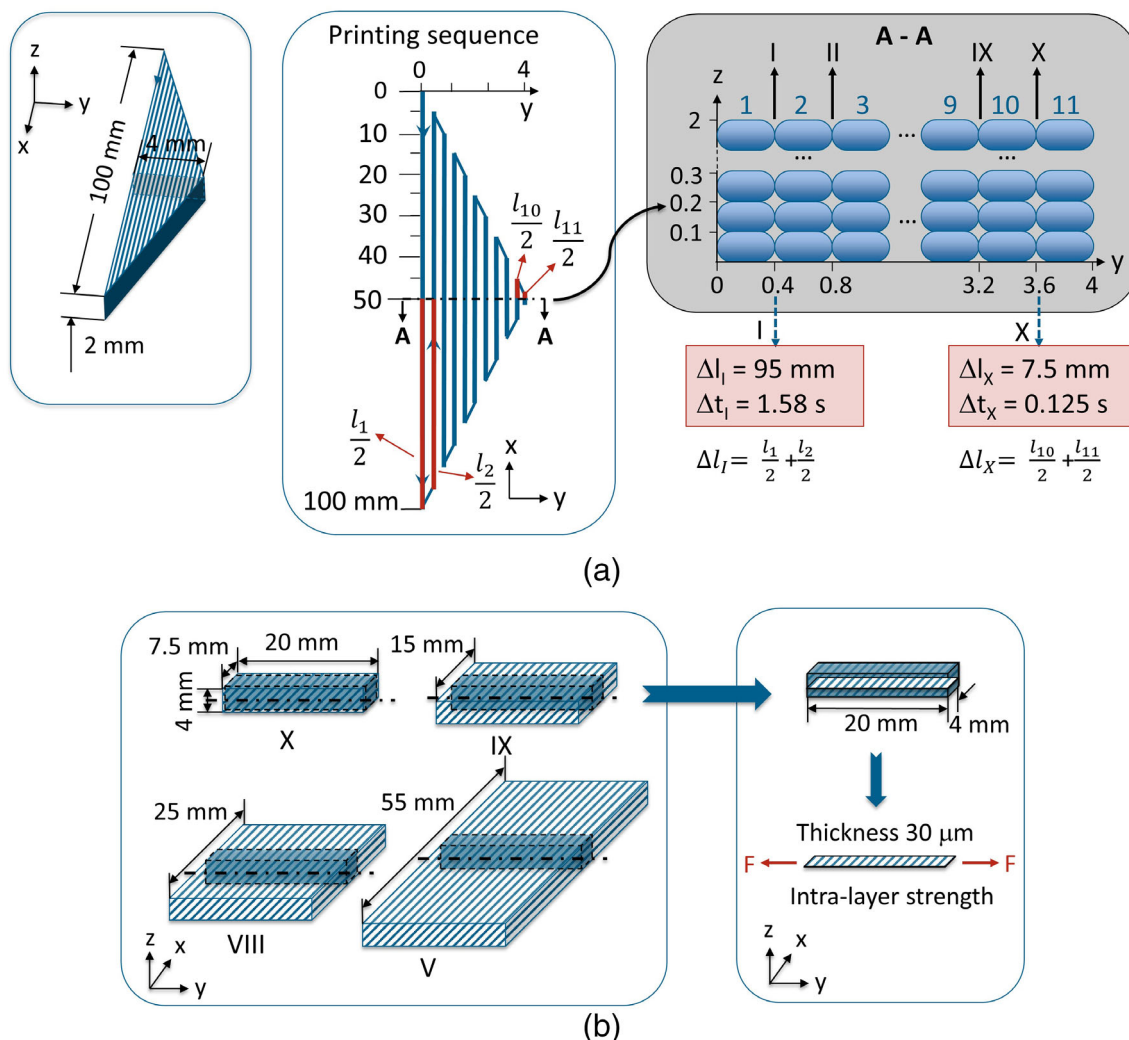$$X_c = \frac{\Delta H_m}{\Delta H_m^\circ} \times 100\% \tag{3}$$

FIGURE 1 Schematic illustration of sample preparation; (a) triangular-shaped specimens, (b) cubic specimens. The strands were numbered from 1 to 11 and the fusion line (interface area) between two adjacent strands were numbered from I to X [Color figure can be viewed at wileyonlinelibrary.com]

TABLE 1 Summary of the 3D printing parameters of all specimens

Sample	Nozzle temperature (T_n) °C	Platform temperature (T_p) °C	Printing speed (v) mm/s	Layer thickness (L_h) mm	Infill %
$T_n = 200°C$	200	60	60	0.1	100
$T_n = 220°C$	220	60	60	0.1	100
$T_n = 240°C$	240	60	60	0.1	100

TABLE 2 Summary of the calculated values for the fusion line of two adjacent strands

Case	I	II	III	IV	V	VI	VII	VIII	IX	X
Δl	95	85	75	65	55	45	35	25	15	7.5
Δt	1.58	1.42	1.25	1.08	0.91	0.75	0.58	0.42	0.25	0.125

where ΔH_m is the measured melting enthalpy, and ΔH_m° is the theoretical specific enthalpy of completely crystallized PP (207 J/g) according to Van Der Wal et al.[33]

During the FFF process, the temperature evolutions as a function of printing time were measured using an ultra-thin K-type thermocouple with 0.1 mm diameter,

which was embedded at the height $z = 0.2$ mm after printing the second layer during the printing processes. The temperature data were recorded and analyzed through a high-frequency analog-digital converter (1000 Hz), amplifier and software Labview 9.0.

For preparing the tensile specimens, inter-strand thin sections of the xy-plane with a thickness of 30 μm were cut by a rotation microtome from the middle part of the cubic specimen as shown in Figure 1b. The tensile testing direction (y-direction, cf. Figure 1b) was perpendicular to the printing direction, which means the inter-strand strength dominates the tensile strength. Micro-tensile tests of the thin section samples (Figure 1b) were conducted on a micro-tensile machine (Kammrath & Weiss GmbH, Dortmund, Germany). The crosshead speed was set at 20 μm/s for stretching with the aid of a template. Meanwhile, the mechanical deformation of the sample was recorded by a charged-coupled device (CCD) camera of an optical microscope.

3 | RESULTS AND DISCUSSION

3.1 | Supermolecular morphology

The morphology of a chemically etched cross-section of the printed triangular-shaped specimen (cf. Figure 1a, cut A-A) is shown in Figure 2. First of all, it is noted that vertical welds, i.e., inter-strand welds are formed between two overlapping adjacent strands in a layer. In the images, it is clear that the vertical welds are less sharp from left to right, i.e., from the long to the short time spans. Considering the finding of Ref. 18, the invisible weld line revealed a higher interfacial diffusion depth, thus, significantly elevated properties. It is indicated that the diffusion depth is considerably increasing with the decrease of the time spans. In addition, the vertical welds are more sharply defined for the sample with a lower nozzle temperature than for the sample with a higher nozzle temperature.
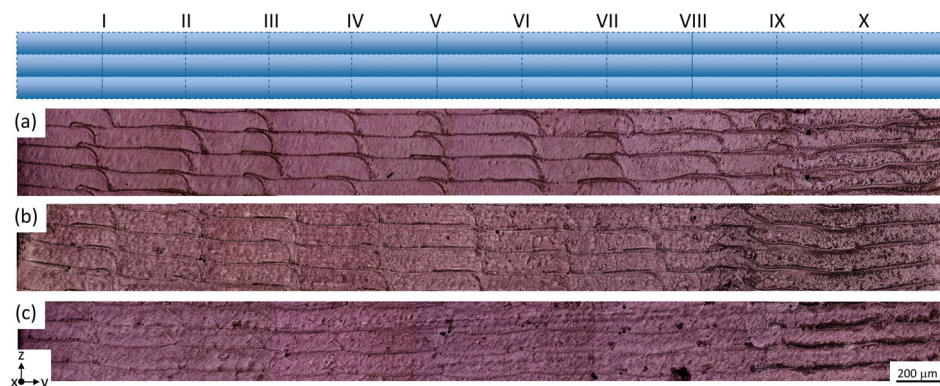
A close view of the morphology shows the oriented supermolecular structures, which are formed at the weld region and perpendicular to the weld line (Figure 3). The oriented structure along the vertical weld lines appeared predominantly in specimens printed with lower nozzle temperature, such as observed in the specimen $T_n = 200°C$ (Figure 3a), by a mechanism as described in Ref. 20. In contrast to this, in the specimen $T_n = 240°C$ (Figure 3c), a less oriented supermolecular morphology is observed along the vertical weld lines. It implied that interfacial merging at the weld lines might be better achieved between strands at higher nozzle temperatures.

3.2 | Thermal analyses

Figure 4 shows the plots of the first heating curves of the DSC measurements for the samples with different fusion lines. The crystallinity has been calculated using Equation (3), and the results are presented in Table 3. It appears that all specimens apart from case V demonstrate double peaks of β-phase at 145°C (β-modification[34,35]) and 155°C (β′-modification due to recrystallization[36]). During the DSC measurements, β-α recrystallization might be occurred.[35]

For any given case, the melting enthalpy of β-crystals is much higher in PP processed at a lower nozzle temperature. The degree of crystallinity (X_c) is slightly lower in the specimen with the lower nozzle temperature. However, the X_c is less sensitive to the time spans in the 3D printed specimen. And it is important to point out that the enthalpy of β-phase of short time spans is higher than that of the long-time spans. It can be concluded that the time spans and nozzle temperature play an important role in the morphology and crystallization behavior, which are presumably due to the complex temperature history during the process.[37] Therefore, the local temperature profile during printing is discussed in the following.

FIGURE 2 Optical micrographs of polypropylene (PP) specimen cross-section surface (cut A-A) (a) $T_n = 200$, (b) $T_n = 220$ and (c) $T_n = 240$ °C. the printing sequence is from I to X. the printing direction is along the x-axis [Color figure can be viewed at wileyonlinelibrary.com]
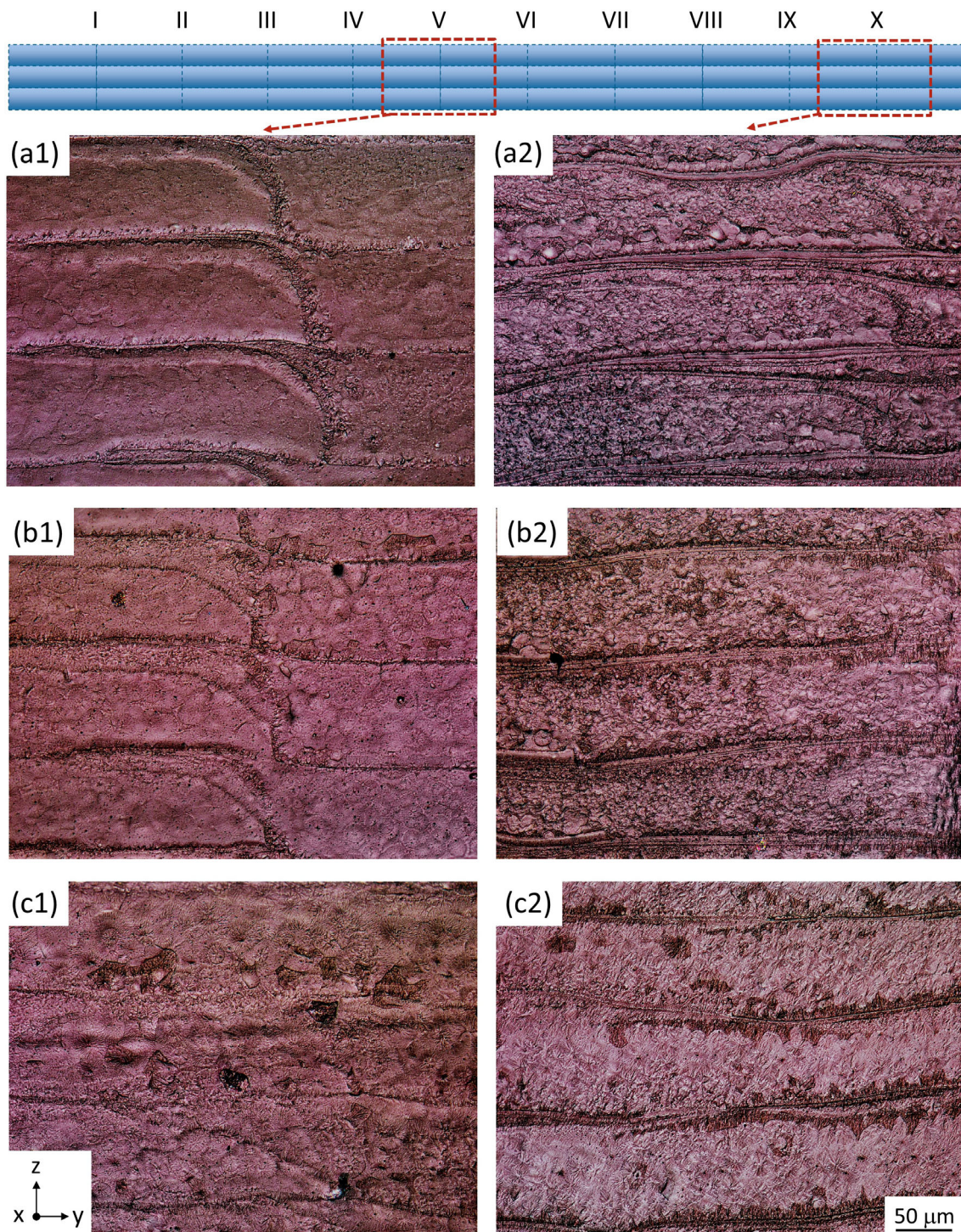
FIGURE 3 Optical micrographs of cross-section (cut A-A) at fusion line (1) V and (2) X of specimens (a) $T_n = 200$, (b) $T_n = 220$ and (c) $T_n = 240°$C. the printing direction is along the x-axis [Color figure can be viewed at wileyonlinelibrary.com]

3.3 | Temperature investigations

Figure 5 shows the temperature profiles of different locations at the height $z = 0.2$ mm of the triangular-shaped specimen. The temperature profile of the print strand ($S_{p,1}$) of 100 mm was shown by the first blue line. In this profile, $t = 0$ s refers to the time when the strand was deposited directly above the position, where the thermocouple was fixed. Once deposited, the strand cools to a temperature $T_{dep,1}$ during the time Δt_I before the deposition of a new adjacent strand. As the next strand of 90 mm is deposited with the extrusion temperature $T_{ext,2}$,

the hot strand transfers heat partially to the neighboring strands previously deposited. In addition, inter-strand interfaces are formed. Therefore, according to the temperature profile, contact temperature $T_{cont,i}$ was calculated by
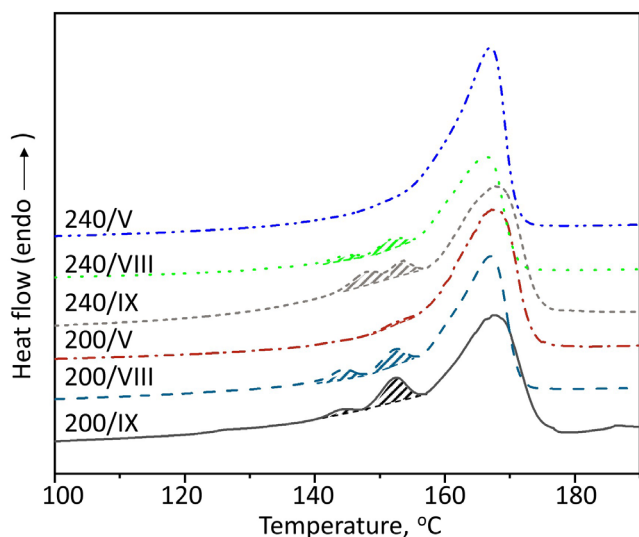
$$T_{cont,i} = (T_{dep,i} + T_{ext,i})/2 \qquad (4)$$

When the material flow is deposited on the short paths (5 mm), the previous strand (10 mm) is still semi-melting,[38] as shown in Figure 5 with $T_{dep,10}$ of 148.2°C. Whereas $T_{dep,1}$ of 100 mm strand is 77.1°C. It can be seen that $T_{dep,i}$ depends on Δt_i between the deposition of the adjacent strands. A prolonged time spans is associated with the length of the printing path and the printing speed, as shown in Table 2. Therefore, the length of the printing path through the time spans affects the $T_{dep,i}$ and consequently the $T_{cont,i}$.

The influence of the time spans on the contact temperature is illustrated in Figure 6. Firstly, increasing the nozzle temperature shifts all of the temperature profiles upwards, resulting in higher crystallinity. The result shows that the contact temperature increased with the decreasing time spans, which can be revealed that more heat is transferred to the weld interface between the part with short time spans, resulting in the invisible weld lines (Figure 3) agreeing well with Ref. 32. It can be inferred that the specimen of shorter time spans has a higher

FIGURE 4 Differential scanning calorimetry (DSC) curves of the polypropylene (PP) specimens on the different process conditions (nozzle temperature/interface case) [Color figure can be viewed at wileyonlinelibrary.com]

TABLE 3 The degree of crystallinity (X_c) and the melting enthalpy of β-phase ($\Delta H_{\beta-phase}$) of the PP specimens on the different process conditions (nozzle temperature and interface case)

Process condition Locations	$T_n = 240°C$			$T_n = 200°C$		
	V	VIII	IX	V	VIII	IX
X_c, %	42.24	42.58	42.49	40.12	42.03	42.09
$\Delta H_{\beta-phase}$, J/g	—	2.33	4.59	0.12	4.70	5.18

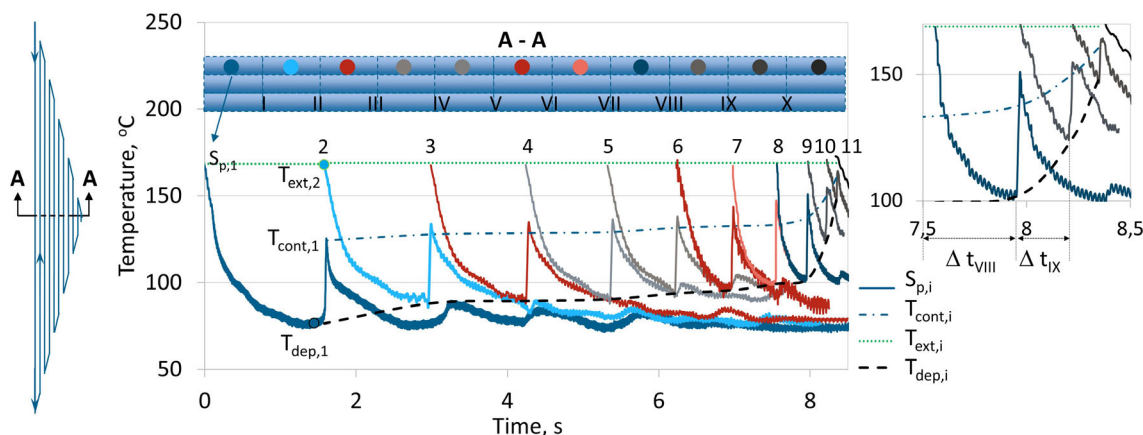Abbreviation: PP, polypropylene.

FIGURE 5 Temperature profiles as a function of time of specimen with the nozzle temperature 200°C [Color figure can be viewed at wileyonlinelibrary.com]

diffusion depth of the interface, which exerts a positive influence on the bonding strength.

3.4 | Mechanical properties

To analyze the influence of the time spans on inter-strand bonding properties, micro-tensile tests were performed. In Figure 7, the influence of the time spans on the tensile strength can be detected. It can be seen that the cubic specimens with shorter time spans have a higher bonding strength. In practically, the specimens with a time span of 0.125 s were up to 32.1% and 18.7%
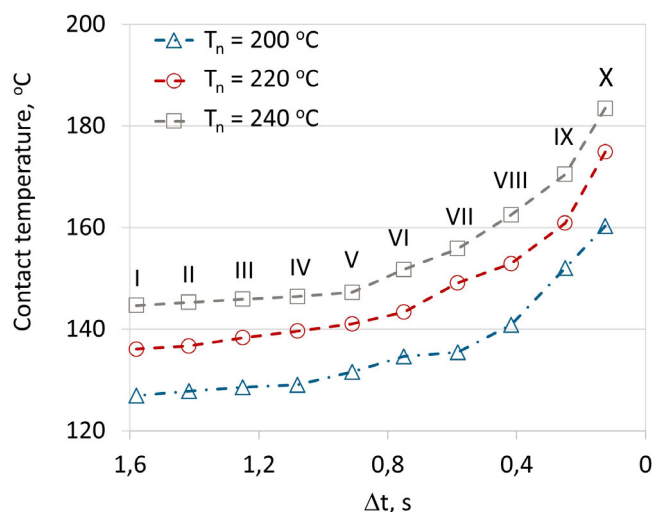
higher than those with the time span of 0.91 s and IM PP, respectively. And the difference is also discernible in the elongation at break. Besides, the 3D specimen with a shorter time span exhibits a significantly higher toughness compared to the specimen with a longer time span, as shown in Figure 7b. The higher toughness can be attributed to the improved inter-diffusion of the specimen under short time span and thus higher contact temperature, which was revealed by the development of micro-crack along with the entire specimen during the micro-tensile tests (Figure 8). The 3D printed samples processed at the longer time span and thus lower contact temperature display significantly crack initiation in the welded joint between the strands (Figure 8b), whereas the one at the shorter time span with higher contact temperature appears clearly visible plastic deformations (Figure 8c). The higher deformation capacity (Figure 8c) is due to improved interdiffusion during material coalescence and a smoother transition between the inner strand material and the weld zone at a short time period and thus higher contact temperature compared to Figure 8b. Although the strength level under optimum processing conditions is comparable to that of the IM specimens, the printed specimen deforms inhomogeneously, i.e., the deformation is triggered and mainly concentrated in the inter-strand weld zones while it is homogeneous in the IM specimens (Figure 8a).

The plot of the tensile strength as a function of the contact temperature in the weld area of 3D printed samples provides attractive results, as shown in Figure 9. As is seen, the tensile strength of 3D printed PP exhibits a quasi-enhancing tendency with increasing contact temperature. When the contact temperatures are above the melt temperature of PP 160°C, a plateau of high tensile
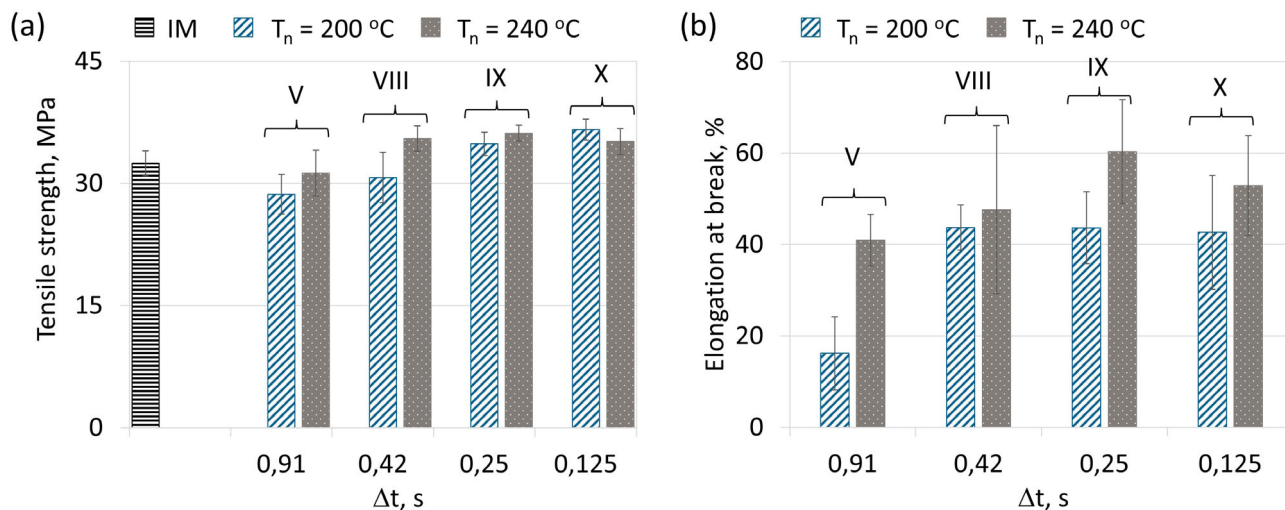

FIGURE 6 Contact temperatures as a function of time spans of specimen with different nozzle temperatures [Color figure can be viewed at wileyonlinelibrary.com]

FIGURE 7 Comparison of (a) tensile strength and (b) elongation at break of thin sections [Color figure can be viewed at wileyonlinelibrary.com]
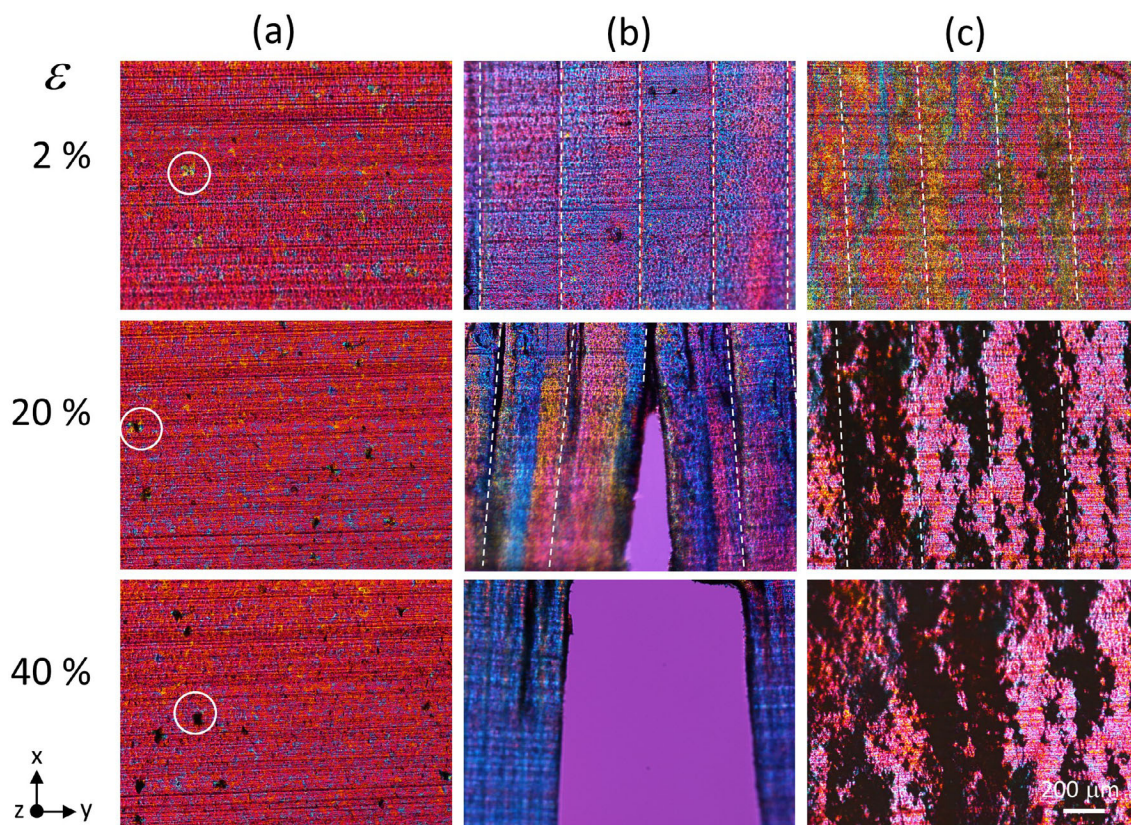
FIGURE 8 Optical micrographs of the polypropylene (PP) inter-strand slices during the micro-tensile tests at elongation of 2%, 20% and 40%. (a) Injection molding plate and 3D printed specimen with different process conditions: (b) 200/V (c) 240/IX (nozzle temperature/ interface case) [Color figure can be viewed at wileyonlinelibrary.com]
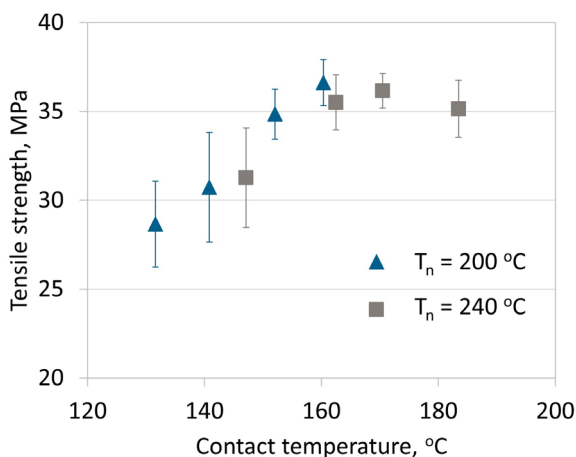

FIGURE 9 Tensile strength as a function of contact temperature of the specimen with different nozzle temperatures [Color figure can be viewed at wileyonlinelibrary.com]

strength can be observed. In order to obtain higher inter-face strengths, the contact temperature is close to the melting temperature of PP, which enables at least short-term melting of the weld areas.[39]

4 | CONCLUSIONS

The work represents an experimental investigation of the effect of the local contact temperature (as a result of a combination of nozzle temperature and time span between the previous and the currently deposited strand) on the morphology, crystallization, and thus inter-strand strength of 3D printed test specimens.

1. The supermolecular structure in the cross-section of the printed specimens revealed by chemical etching shows that shorter time spans between strand contact produce less pronounced weld lines.
2. At the same nozzle temperature and shorter time to contact between two deposited strands, this contact occurs at a higher temperature.
3. Microtensile tests showed that both the tensile strength increases with increasing contact temperature and reaches a constant level in the range of the melting temperature of the material, and that crack initiation in the welded joint between the strands decreases significantly with increasing contact temperature.

Overall, it was thus possible to demonstrate that PP components can be produced at injection molding level with FFF if the right printing design is selected. Further investigations, in conjunction with thermal simulations, should show how other parameters, such as platform temperature, layer height, throughput, etc., affect the contact temperature, and thus ultimately the mechanical properties. If these relationships are known, the slicing strategy can be modified for a given component design so that the mechanical performance potential of the material can be fully exploited.

AUTHOR CONTRIBUTIONS
Yao Xu: Investigation (lead); project administration (equal); writing – original draft (equal). **Miaozi Huang:** Project administration (equal); validation (lead); writing – original draft (supporting). **Alois K. Schlarb:** Conceptualization (lead); funding acquisition (lead); supervision (lead); writing – review and editing (lead).

DATA AVAILABILITY STATEMENT
Research data are not shared.

ORCID
Alois K. Schlarb https://orcid.org/0000-0001-8693-9163

REFERENCES
[1] N. Guo, M. C. Leu, *Front. Mech. Eng.* **2013**, *8*, 215.

[2] M. Gebler, A. J. M. Schoot Uiterkamp, C. Visser, *Energy Policy* **2014**, *74*, 158.

[3] D. Bourell, D. Espalin, K. Arcaute, D. Rodriguez, F. Medina, M. Posner, R. Wicker, *Rapid Prototyp. J.* **2010**, *16*, 164.

[4] M. Z. Huang, Y. Xu, A. K. Schlarb, *J. Appl. Polym. Sci.* **2021**, *138*, 50557.

[5] S.S. Crump, US Pat. US5121329A, 1989.

[6] J. Yin, C. Lu, J. Fu, Y. Huang, Y. Zheng, *Mater. Des.* **2018**, *150*, 104.

[7] A. Paolini, S. Kollmannsberger, E. Rank, *Addit. Manuf.* **2019**, *30*, 100894.

[8] S. Bakrani Balani, F. Chabert, V. Nassiet, A. Cantarel, *Addit. Manuf.* **2019**, *25*, 112.

[9] G. D. Goh, Y. L. Yap, S. Agarwala, W. Y. Yeong, *Adv. Mater. Technol.* **2019**, *4*, 1.

[10] C. Kousiatza, D. Karalekas, *Mater. Des.* **2016**, *97*, 400.

[11] D. Drummer, S. Cifuentes-Cuéllar, D. Rietzel, *Rapid Prototyp. J.* **2012**, *18*, 500.

[12] C. Kousiatza, N. Chatzidai, D. Karalekas, *Sensors* **2017**, *17*, 456.

[13] Y. Shmueli, J. Jiang, Y. Zhou, Y. Xue, C.-C. Chang, G. Yuan, S. K. Satija, S. Lee, C.-Y. Nam, T. Kim, G. Marom, D. Gersappe, M. H. Rafailovich, *ACS Appl. Polym. Mater.* **2019**, *1*, 1559.

[14] X. Gao, S. Qi, X. Kuang, Y. Su, J. Li, D. Wang, *Addit. Manuf.* **2021**, *37*, 101658.

[15] M. Albrecht, A. K. Schlarb, *Zeitschrift Kunststofftechnik* **2016**, *3*, 185.

[16] N. P. Levenhagen, M. D. Dadmun, *Polymer* **2018**, *152*, 35.

[17] X. Peng, S. Liu, Y. Huang, L. Sang, *Int. J. Adhes. Adhes.* **2020**, *100*, 102615.

[18] S. Petersmann, P. Spoerk-Erdely, M. Feuchter, T. Wieme, F. Arbeiter, M. Spoerk, *Addit. Manuf.* **2020**, *35*, 101384.

[19] G. Bräuer, K. Sachsenhofer, R. W. Lang, *Addit. Manuf.* **2021**, *46*, 102105.

[20] Y. Shmueli, Y. C. Lin, S. Lee, M. Zhernenkov, R. Tannenbaum, G. Marom, M. H. Rafailovich, *ACS Appl. Mater. Interfaces* **2019**, *11*, 37112.

[21] V. Srinivas, C. S. J. van Hooy-Corstjens, J. A. W. Harings, *Polymer* **2018**, *142*, 348.

[22] N. P. Levenhagen, M. D. Dadmun, *Polymer* **2017**, *122*, 232.

[23] L. J. Tan, W. Zhu, K. Zhou, *Adv. Funct. Mater.* **2020**, *30*, 2003062.

[24] Y. Liao, C. Liu, B. Coppola, G. Barra, L. Di Maio, L. Incarnato, K. Lafdi, *Polymers* **2019**, *11*, 1.

[25] L. Wang, W. M. Gramlich, D. J. Gardner, *Polymer* **2017**, *114*, 242.

[26] Y. Lyu, H. Zhao, X. Wen, L. Lin, A. K. Schlarb, X. Shi, *J. Appl. Polym. Sci.* **2021**, *138*, 1.

[27] N. Aliheidari, R. Tripuraneni, C. Hohimer, J. Christ, A. Ameli, S. Nadimpalli, *Behav. Mech. Multifunct. Mater. Compos.* **2017**, *10165*, 1016512.

[28] X. Zhang, J. Wang, *Chem. Phys. Lett.* **2020**, *739*, 136959.

[29] D. P. Cole, J. C. Riddick, H. M. Iftekhar Jaim, K. E. Strawhecker, N. E. Zander, *J. Appl. Polym. Sci.* **2016**, *133*, 1.

[30] M. Spoerk, J. Gonzalez-Gutierrez, J. Sapkota, S. Schuschnigg, C. Holzer, *Plast. Rubber Compos.* **2018**, *47*, 17.

[31] C. S. Davis, K. E. Hillgartner, S. H. Han, J. E. Seppala, *Addit. Manuf.* **2017**, *16*, 162.

[32] S. Hertle, M. Drexler, D. Drummer, *Macromol. Mater. Eng.* **2016**, *301*, 1482.

[33] A. Van Der Wal, J. J. Mulder, R. J. F. Gaymans, *Polymer* **1998**, *39*, 5477.

[34] J. Varga, *J. Mater. Sci.* **1992**, *10*, 2557.

[35] J. Varga, *J. Macromol. Sci.-Phys.* **2002**, *41*, 1121.

[36] Y. Fujiwara, *Colloid Polym. Sci.* **1975**, *253*, 273.

[37] C. McIlroy, P. D. Olmsted, *Polymer* **2017**, *123*, 376.

[38] B. Suksut, *Morphology and Morphology Formation of Injection Molded PP-based Nanocomposites*, Technische Universität Kaiserslautern, Kaiserslautern, Germany **2016**.

[39] Q. Sun, G. M. Rizvi, C. T. Bellehumeur, P. Gu, *Rapid Prototyp. J.* **2008**, *14*, 72.

How to cite this article: Y. Xu, M. Huang, A. K. Schlarb, *J. Appl. Polym. Sci.* **2022**, *139*(24), e52337. https://doi.org/10.1002/app.52337